Characterization of the transcriptional response of Candida parapsilosis to the antifungal peptide MAF-1A

Rong Cheng[1], Wei Li[2], Klarke M. Sample[3,4], Qiang Xu[3,4], Lin Liu[4,5], Fuxun Yu[3,4], Yingjie Nie[3,4], Xiangyan Zhang[4,5] and Zhenhua Luo[3,4]

[1] Guizhou University School of Medicine, Guiyang, China
[2] Department of Cadiovascular Medicine, Affiliated Hospital of Guizhou Medical University, Guiyang, China
[3] Department of Central Lab, Guizhou Provincial People's Hospital, Guiyang, China
[4] NHC Key Laboratory of Pulmonary Immune-related Diseases, Guizhou Provincial People's Hospital, Guiyang, China
[5] Department of Respiratory and Critical Care Medicine, Guizhou Provincial People's Hospital, Guiyang, China

ABSTRACT

Candida parapsilosis is a major fungal pathogen that leads to sepsis. New and more effective antifungal agents are required due to the emergence of resistant fungal strains. MAF-1A is a cationic antifungal peptide isolated from Musca domestica that is effective against a variety of Candida species. However, the mechanism(s) of its antifungal activity remains undefined. Here, we used RNA-seq to identify differentially expressed genes (DEGs) in Candida parapsilosis following MAF-1A exposure. The early (6 h) response included 1,122 upregulated and 1,065 downregulated genes. Late (18 h) responses were associated with the increased expression of 101 genes and the decreased expression of 151 genes. Upon MAF-1A treatment for 18 h, 42 genes were upregulated and 25 genes were downregulated. KEGG enrichment showed that the DEGs in response to MAF-1A were mainly involved in amino acid synthesis and metabolism, oxidative phosphorylation, sterol synthesis, and apoptosis. These results indicate that MAF-1A exerts antifungal activity through interference with Candida parapsilosis cell membrane integrity and organelle function. This provides new insight into the interaction between Candida parapsilosis and this antimicrobial peptide and serves as a reference for future Candida parapsilosis therapies.

Subjects Bioinformatics, Genomics, Microbiology, Molecular Biology, Mycology
Keywords Antimicrobial peptide, Antifungal, MAF-1A, Candida parapsilosis, Transcriptional response, RNA-seq

INTRODUCTION

Immunosuppressed patients are at a high risk of hospital-acquired fungal infections. Candida albicans (C. albicans) is the most common pathogen of Candida species, its dominance has decreased as the incidence of non-albicans Candida (NAC) species have increased (*Vieira de Melo et al., 2019*). Over the last two decades, epidemiological studies of fungal pathogens have shown that NAC has surpassed C. albicans as the most prevalent cause of invasive Candida (*Sular et al., 2018*). New anti-NAC treatment regimens are therefore urgently required.

Submitted 10 February 2020
Accepted 29 July 2020
Published 7 September 2020

Corresponding authors
Xiangyan Zhang, zxiangyan12@sina.com
Zhenhua Luo, luo8300@sina.com

Academic editor
Timothy Read

Additional Information and Declarations can be found on page 14

DOI **10.7717/peerj.9767**

Amongst NAC infections, Candida parapsilosis (C. parapsilosis) is particularly problematic due to its propensity to form biofilms on central venous catheters and other medically implanted devices (*Fais et al., 2017*; *Vieira de Melo et al., 2019*). Additionally, patients in the intensive care unit (ICU) who have undergone total parenteral nutrition are highly susceptible to C. parapsilosis infection, including undernourished children and neonates of low-birth-weights. Recent epidemiological studies have shown that C. parapsilosis is the second most commonly isolated species following only C. albicans in southern Europe, some regions of Asia, and Latin America (*Toth et al., 2019*). When immunosuppressed patients are exposed to C. parapsilosis, the rate of infection is high. The biological characteristics of infection, include toxicity, immune regulation, and drug resistance are in contrast with those of C. albicans (*Toth et al., 2019*). These interspecies specificities affect recognition by the host, clearance, and antifungal drug efficacy.

Candida pathogens have developed varying degrees of drug resistance, with some representing a serious threat to human health (*Robbins, Caplan & Cowen, 2017*). The currently available antifungal agents inhibit cell wall synthesis (echinocandins), destroy cell membrane components (azoles), or bind to ergosterol and perforate the cell membrane (amphotericin B). With the widespread use of antifungal drugs, the presence of drug resistance-related genes has increased. Antimicrobial peptides (AMPs) form a key arm of the innate immune response of a variety of organisms including plants, insects, and humans (*Moravej et al., 2018*). It is uncommon for microbial infections to be resistant to AMPs which are an emerging source of novel antifungal drugs (*Ghosh et al., 2019*; *Nuti et al., 2017*; *Patocka et al., 2018*), making these molecules a potential alternative to fungemia therapies.

AMPs can exhibit both cationic and amphiphilic properties. Cationic AMPs are amphipathic permitting their interaction with negatively charged cell membranes, leading to cell membrane disruption and cell death (*Kobbi et al., 2018*). AMPs are diverse with respect to length (20–100 amino acids), sequence and structure, and are produced by almost all organisms. Filamentous fungi produce a wide spectrum of AMPs that serve as defense and/or host signaling molecules. Penicillium chrysogenum secretes PAF and PAFB that possess complex tertiary structures and activity centers. PAF and PAFB are produced as 92 amino acid preproproteins that are active against a variety of pathogenic fungi, bacteria, and viruses (*Huber et al., 2020*). Insects are extremely resistant to microbial infections, which are an important source of AMPs. Insect AMPs are smaller (between 12 and 50 amino acids) with secondary structures formed predominantly of α-helices and β-sheets. Whilst membrane damage is the canonical mechanism through which AMPs act, other mechanisms exist. AMPs have specific subcellular targets, including the inhibition of DNA synthesis, RNA synthesis, protein synthesis, and cell wall integrity (*Guilhelmelli et al., 2013*; *Li et al., 2016*). However, their mechanism(s) of action at the molecular level remain unclear. The Musca domestica antifungal peptide-1 (MAF-1) is a novel cationic AMP isolated from the instar larvae of houseflies (*Fu, Wu & Guo, 2009*). We previously cloned the full-length MAF-1 gene and derived 26 amino acid MAF-1A peptides from the MAF-1 structural domain. Despite the established antifungal effects of MAF-1A, the molecular mechanism(s) governing its activity remain largely undefined (*Zhou et al., 2016*).

In recent years, the development of high throughput sequencing technologies has facilitated research on both antimicrobial drug function and drug-resistance. For example, HAC1 (CPAR2_103720) is a key mediator of endoplasmic reticulum stress in C. parapsilosis identified through RNA-seq (*Iracane et al., 2018*). In our previous studies, we showed that MAF-1A inhibits C. albicans through its effects on the cell wall, plasma membrane, protein synthesis, and energy metabolism (*Wang et al., 2017*). However, the mechanism(s) through which C. albicans responds to MAF-1A were not fully defined. Here, we have expanded our knowledge on how MAF-1A acts on C. parapsilosis and investigated differences in the responses of C. albicans and C. parapsilosis to MAF-1A treatment. RNA-seq was used to investigate changes in gene expression at early (6 h) and late (18 h) time points, according to time-kill curves of C. parapsilosis growth.

MATERIALS AND METHODS

Strains and growth conditions

Transcriptional profiling was performed on the C. parapsilosis reference strain ATCC22019. The strain was preserved in goat blood and stored at −80 °C. C. parapsilosis was streaked on Sabouraud Dextrose Agar (SDA) plates (Sangon, Shanghai, China) at 35 °C as described by *Lis et al. (2010)*. MAF-1A treatments were performed in Sabouraud Dextrose Broth (SDB) (Sangon, Shanghai, China).

Peptide synthesis

MAF-1A was synthesized by Sangon Biotech (Shanghai, Shanghai, China) as a linear peptide of 26 amino acids: KKFKETADKLIESAKQQLESLAKEMK. Analytical high-performance liquid chromatography (HPLC) was used to confirm purity $\geq$ 95%. The peptide was dissolved in sterile ultrapure water at 5 mg/mL and stored at −20 °C.

Minimum inhibitory concentration (MIC) and time-kill curves

Antifungal assays were performed as per the requirements of the Clinical and Laboratory Standards Institute (CLSI) M27-A3. Briefly, cultures were grown for 24 h at 35 °C and resuspended in SDB. Concentrations were adjusted to approximately 0.5×10^3–2.5×10^3 CFU/mL and 100 µl of the suspension was added to each well of 96-well polypropylene microplates (NEST, Wuxi, China). MAF-1A was added at concentration ranging from 0.1 mg/mL to 1.2 mg/mL. All experiments were performed in triplicates. After incubation at 35 °C for 24 h, absorbances were measured at 492 nm on a Microplate Reader (BioTek Synergy H1, Vermont, USA). MIC was defined as the lowest drug concentration showing 80% growth inhibition compared to the drug-free controls. The following formulas were used (*Li et al., 2008*):

(1) Percentage Fungal Growth = (Treatment Well A Value − Control Well A Value)/(Growth in Control Well A Value − Control Well A Value) × 100%.

(2) Percentage Inhibition of Fungal Growth = 1 − Percentage Fungal Growth.

Time-kill curves were performed according to the literature (*Li et al., 2008*; *Sun et al., 2008*). C. parapsilosis suspensions were mixed with MAF-1A (MIC) in triplicate and cultured at 35 °C. Aliquots of 100 µl were removed from each test solution at pre-determined time points (0, 2, 4, 6, 8, 10, 12, 14, 16, 18, 20, 22, and 24 h). Dilutions were

produced (1:100) and streaked in triplicate onto SDA agar plates for colony counts after incubation at 35 °C for 24 h. Sterile ultrapure water was used as a control.

Transcriptome sequencing

C. parapsilosis was inoculated into SDB medium (Sangon, Shanghai, China) at 35 °C for 24 h. C. parapsilosis was treated with MAF-1A at MIC for 6 h (CPAS) and 18 h (CPBS), before RNA extraction. Untreated cultures served as controls (6 h, CPAC; 18 h, CPBC). Total RNA was extracted using RNAiso Plus (Takara, Dalian, China) according to the manufacturer's instructions. RNA concentration and quality were determined on a NanoDrop 2000 (Thermo Fisher Scientific, Wilmington, DE, USA) and Agilent 2100 bioanalyzer (Agilent Technologies, CA, USA). Libraries were prepared using NEBNext® UltraTM RNA Library Prep Kit (NEB, USA) as per the manufacturer's recommendations. Purified libraries were quantified on an Agilent 2100 bioanalyzer Effective concentrations were determined through qRT-PCR analysis. Libraries were prepared and sequenced using a Novoseq sequencer (Illumina, USA) to produce 150 bp paired-end reads.

Differential expression analysis

Raw reads were filtered to obtain high-quality clean reads for subsequent analysis. All reads were mapped to the reference genome of C. parapsilosis (assembly ASM18276v2) from the National Center for Biotechnology Information (NCBI) using HISAT2 v2.0.5 (*Kim, Langmead & Salzberg, 2015*). Differential expression analysis between the conditions was assessed using the Bioconductor software package DESeq2 in R 1.16.1 (*Love, Huber & Anders, 2014*). Relative gene expression was assessed using FPKM (Fragments Per Kilobase of transcript sequence per Millions of base pairs sequenced) and compared using log2 FC. *P*-values were adjusted to generate false discovery rates (padj) as described by Benjamini-Yekutieli, assigning the significance threshold for DEGs as padj < 0.05 (*Benjamini et al., 2001*; *Mortazavi et al., 2008*).

Enrichment and interaction network analysis of the differentially expressed genes

To further understand the functions of the DEGs, Gene Ontology (GO) enrichment was performed using the Bioconductor software clusterProfiler 3.4.4 in R package (*Yu et al., 2012*). Statistical enrichment of the DEGs was also performed in the Kyoto Encyclopedia of Genes and Genomes (KEGG) for pathway enrichment (*Kanehisa et al., 2019*; *Ogata et al., 1999*). PPI analysis of the DEGs was performed based on the STRING database to define key protein-protein interactions (*Yu et al., 2012*). The network was constructed using Cytoscape 3.6.1 (*Shannon et al., 2003*).

Validation of RNA-seq by quantitative RT-PCR (qRT-PCR)

To confirm the RNA-seq data, 20 DEGs (10 with increased expression and 10 with decreased expression) were selected for qRT-PCR validations. Reactions were performed using SYBR Premix Ex Taq TM Kit (Takara) according to the manufacturer's protocol. Reaction conditions were as follows: 40 cycles of 95 °C for 30 s; 95 °C for 5 s; and 60 °C for 30 s. PCRs were performed on a BIO-RAD CFX-Connect Real-Time System. Relative gene

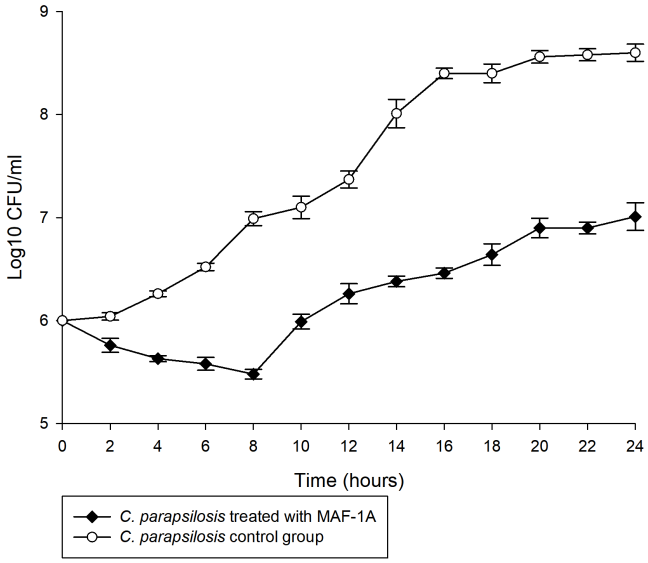

Figure 1 Time-kill curves of MAF-1A under MIC for C. parapsilosis. The mean growth of three C. parapsilosis cultures were recorded (Log10 CFU/ml) every 2 h for 24 h.

Full-size DOI: 10.7717/peerj.9767/fig-1

expression was determined using the $2^{-\Delta\Delta Ct}$ method normalized to 18S rRNA (*Livak & Schmittgen, 2001*). Significant differences were determined using a *t*-test with a threshold of $p < 0.05$. Primers are listed in Table S1. Primer efficiency and melting curves are listed in Table S2 and Figs. S1–S5.

RESULTS

MIC assays and time-kill curves

The MIC of MAF-1A against C. parapsilosis was determined as 0.6 mg/mL. Time-kill curves of MAF-1A at MIC showed a gradual antifungal effect during the first 8 h of C. parapsilosis culture (Fig. 1). After 8 h, cell numbers increased but remained lower than those of the control group.

Transcriptional stress responses and enrichment analysis of MAF-1A treated C. parapsilosis

RNA-seq analysis in C. parapsilosis treated with MAF-1A for 6 and 18 h showed 5,747 DEGs. Sequence reads were deposited in the NCBI Sequence Read Archive (SRA) under accession number PRJNA638006. A total of 2,439 DEGs were detected. Out of these genes, 2187 were identified at 6 h, representing 38.05% of the total detectable genes. A total of 252 genes were differentially expressed after 18 h and accounted for 4.38% of the total expressed genes. After 6 and 18 h of MAF-1A treatment, 67 DEGs with opposite trends were observed (reversed genes 1, RG1 and reversed genes 2, RG2). In total, 56 DEGs were upregulated, whilst down-regulated genes remained unchanged (one unchanged genes: UG1; two unchanged genes: UG2) (Fig. 2).

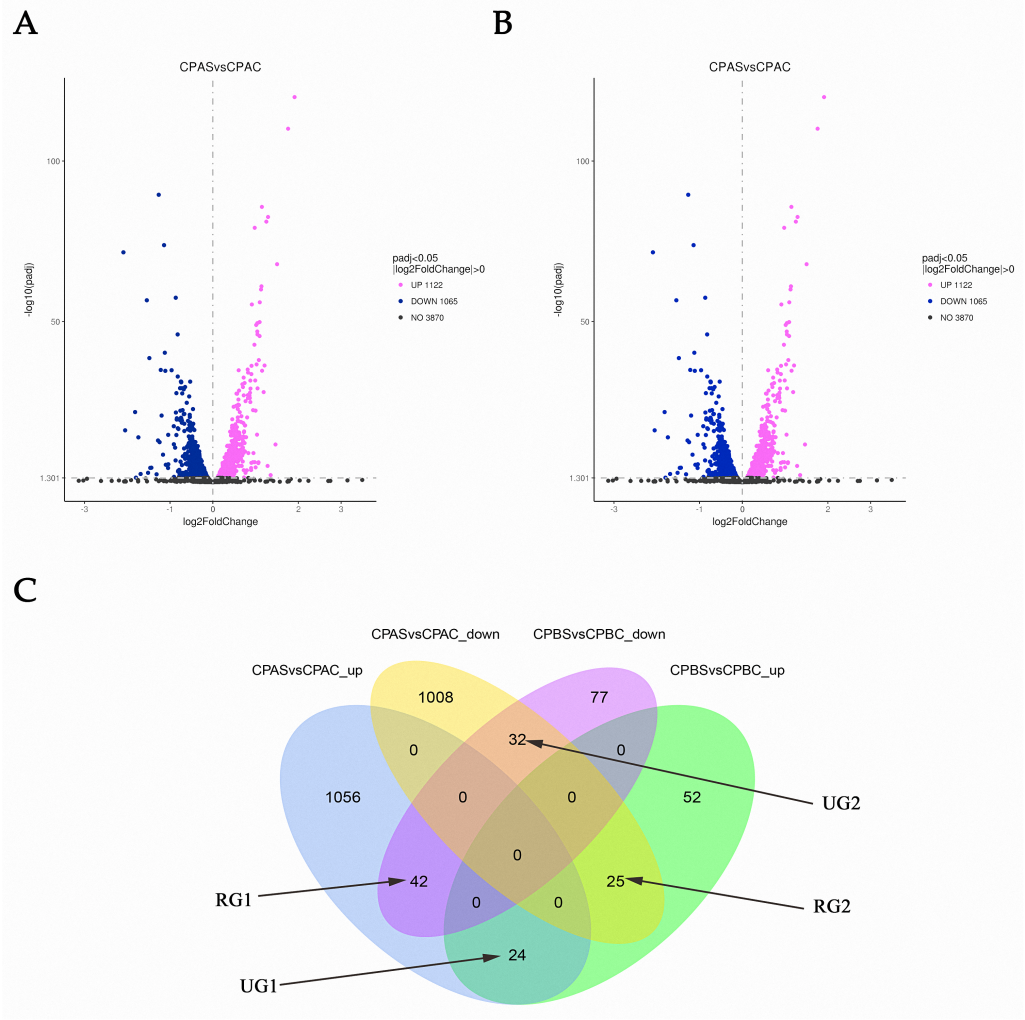

Figure 2 Gene expression changes in C. parapsilosis following MAF-1A treatment. Volcano plots of the DEGs. (A) Volcano plots depicting log2 FC (fold change) in expression after 6 h of treatment with MAF-1A, (C) parapsilosis was treated with MAF-1A at MIC for 6 h (CPAS), without MAF-1A as a control (CPAC). The expression of 1122 genes significantly increased; 1065 genes were significantly downregulated (padj < 0.05). (B) Volcano plot depicting the log2 FC expression after 18 h of treatment with MAF-1A. (C) parapsilosis was treated with MAF-1A at MIC for 18 h (CPBS). Controls lacked MAF-1A treatment (CPBC). The expression of 101 genes significantly increased in contrast to 151 genes whose expression decreased (padj < 0.05). (C) Gene expression Venn diagrams revealing two gene groups with opposite trends, labeled as RG1, RG2, UG1 and UG2; CPAS vs. CPAC_up: genes with increased expression after 6 h; CPAS vs. CPAC down: genes with decreased expression after 6 h; CPBS vs. CPBC_up: genes with increased expression after 18 h; CPBS vs. CPBC down: genes with decreased expression after 18 h.
Full-size DOI: 10.7717/peerj.9767/fig-2

DEG enrichment analysis

Amongst the DEGs at 6 h, 1122 showing increased expression were enriched in 85 KEGG pathways, 20 of which were significant with padj < 0.05. The most significant pathways with increased expression in C. parapsilosis following MAF-1A treatment were: oxidative

Table 1 Significantly enriched KEGG pathways for genes with increased expression after 6 h of MAF-1A treatment.

KEGG ID	Description	*p* value	padj
cdu00190	Oxidative phosphorylation	3.34×10^{-12}	2.84×10^{-10}
cdu04146	Peroxisome	2.02×10^{-8}	8.56×10^{-7}
cdu00020	Citrate cycle (TCA cycle)	2.21×10^{-5}	6.27×10^{-4}
cdu01200	Carbon metabolism	3.50×10^{-5}	7.44×10^{-4}
cdu04111	Cell cycle—yeast	9.20×10^{-5}	1.56×10^{-3}
cdu04011	MAPK signaling pathway—yeast	8.17×10^{-4}	1.16×10^{-2}
cdu04113	Meiosis—yeast	2.35×10^{-3}	2.80×10^{-2}
cdu00071	Fatty acid degradation	2.63×10^{-3}	2.80×10^{-2}
cdu04136	Autophagy—other	4.03×10^{-3}	3.80×10^{-2}

Notes.
padj of < 0.05 set as the significance threshold.

phosphorylation, peroxisome, citrate cycle (TCA cycle), carbon metabolism, cell cycle-yeast, MAPK signaling-yeast, meiosis-yeast, fatty acid degradation, and autophagy (Table 1). Genes of decreased expression were enriched in steroid biosynthesis, biosynthesis of amino acids, cysteine and methionine metabolism, biosynthesis of antibiotics, ribosome, RNA polymerase, biosynthesis of secondary metabolites, RNA transport, ribosome biogenesis in eukaryotes, lysine biosynthesis, 2-oxocarboxylic acid metabolism, pyrimidine metabolism, glycine, serine and threonine metabolism and purine metabolism (Table 2). At 18 h, 101 genes were upregulated and enriched in 24 KEGG pathways, two of which were significant (Table 3). A total of 151 genes were downregulated and significantly enriched in carbon metabolism, biosynthesis of antibiotics, oxidative phosphorylation, the biosynthesis of secondary metabolites, and the biosynthesis of amino acids (Table 4).

RG1, RG2, UG1, and UG2 gene enrichment analysis

The 42 genes in RG1 were enriched in 17 KEGG pathways, of which oxidative phosphorylation was most significant. Additionally, 25 genes in RG2 were enriched in 13 KEGG pathways, of which arginine biosynthesis, the biosynthesis of antibiotics, the biosynthesis of amino acids, and the biosynthesis of secondary metabolites were enriched. A total of 24 genes in UG1 and 32 genes in UG2 were enriched in 8 and 20 KEGG pathways, respectively. In UG1, the genes were enriched in butanoate metabolism, propionate metabolism, beta-alanine metabolism, valine, leucine, and isoleucine degradation. No pathways were significantly enriched in UG2 at a padj < 0.05 (Table 5).

Genes in RG1, RG2, UG1, and UG2 were enriched in 535 GO terms, a total of 9 of which were significant (Table 6). Genes in RG1 were involved in energy production and redox processes. Genes in RG2 were associated with the anabolic processes of various organic acids. Genes in UG2 were involved in oxidation–reduction processes.

Verification of differentially expressed genes

A total of 20 genes were selected, including 10 with increased expression and 10 with decreased expression. Genes were evenly selected from 6 h and 18 h time points to validate the RNA-seq data by qRT-PCR. The results indicated the expression levels have a

Table 2 Significantly enriched KEGG pathways for genes with decreased expression after 6 h of MAF-1A treatment.

KEGG ID	Description	*p* value	padj
cdu00100	Steroid biosynthesis	1.64×10^{-8}	1.40×10^{-6}
cdu01230	Biosynthesis of amino acids	5.95×10^{-7}	2.53×10^{-5}
cdu00270	Cysteine and methionine metabolism	4.80×10^{-6}	1.36×10^{-4}
cdu01130	Biosynthesis of antibiotics	1.07×10^{-5}	2.27×10^{-4}
cdu03010	Ribosome	3.01×10^{-5}	5.12×10^{-4}
cdu03020	RNA polymerase	2.14×10^{-4}	3.03×10^{-3}
cdu01110	Biosynthesis of secondary metabolites	3.68×10^{-4}	4.47×10^{-3}
cdu03013	RNA transport	9.34×10^{-4}	8.83×10^{-3}
cdu03008	Ribosome biogenesis in eukaryotes	9.35×10^{-4}	8.83×10^{-3}
cdu00300	Lysine biosynthesis	2.31×10^{-3}	1.96×10^{-2}
cdu01210	2-Oxocarboxylic acid metabolism	2.66×10^{-3}	2.05×10^{-2}
cdu00240	Pyrimidine metabolism	3.54×10^{-3}	2.40×10^{-2}
cdu00260	Glycine, serine and threonine metabolism	3.67×10^{-3}	2.40×10^{-2}
cdu00230	Purine metabolism	5.08×10^{-3}	3.09×10^{-2}

Notes.
padj of < 0.05 set as the significance threshold.

Table 3 Significantly enriched KEGG pathways for genes with increased expression after 18 h of MAF-1A treatment.

KEGG ID	Description	*p*-value	padj
cdu00220	Arginine biosynthesis	3.01×10^{-4}	7.21×10^{-3}
cdu00250	Alanine, aspartate and glutamate metabolism	1.48×10^{-3}	1.77×10^{-2}

Notes.
padj of < 0.05 were set as the significance threshold.

consistent change for both RNASeq and qRT-PCR. Hence, the qRT-PCR results confirmed the reliability of our RNA-Seq data (Fig. 3).

Protein-protein interaction (PPI) network analysis

We constructed a PPI network based on the STRING database of the DEGs after 6 h of treatment. The PPI network contained 624 nodes and 6264 edges, with a degree filter of ≥ 10 (Fig. 4). The connectivity degree (dg) of multiple nodes in the PPI network were high, including: CpUbi1 (dg = 146), CpGlt1 (dg = 82), CpCdc28 (dg = 54), CpCys4 (dg = 50), CpCyt1 (dg = 45), CpRpc40 (dg = 42), CpArx1 (dg = 42), CpDim1 (dg = 41), CpYtm1 (dg = 41), CpRip1 (dg = 41). Upon enrichment analyses the identified genes were associated with oxidative phosphorylation (Fig. S6).

DISCUSSION

C. parapsilosis is one of the most prevalent fungal species in many regions. In addition to its high rates of infection, its etiology differs from that of C. albicans (*Holland et al., 2014*). Specific C. parapsilosis isolates are resistant to conventional antifungal drugs including echinocandins, azoles, and amphotericin B (*Lotfali et al., 2016*; *Maria et al., 2018*; *Thomaz et al., 2018*). Antimicrobial peptides lead to cell lysis and death through

Table 4 Significantly enriched KEGG pathways for genes with decreased expression after 18 h of MAF-1A treatment.

KEGG ID	Description	*p*-value	padj
cdu01200	Carbon metabolism	1.65×10^{-8}	7.61×10^{-7}
cdu01130	Biosynthesis of antibiotics	6.21×10^{-7}	1.43×10^{-5}
cdu00190	Oxidative phosphorylation	5.58×10^{-6}	6.91×10^{-5}
cdu01110	Biosynthesis of secondary metabolites	6.01×10^{-6}	6.91×10^{-5}
cdu00010	Glycolysis/Gluconeogenesis	1.71×10^{-5}	1.57×10^{-4}
cdu00260	Glycine, serine and threonine metabolism	5.83×10^{-4}	4.47×10^{-3}
cdu01230	Biosynthesis of amino acids	1.77×10^{-3}	1.16×10^{-2}
cdu00680	Methane metabolism	3.62×10^{-3}	2.05×10^{-2}
cdu00520	Amino sugar and nucleotide sugar metabolism	4.02×10^{-3}	2.05×10^{-2}
cdu00052	Galactose metabolism	6.24×10^{-3}	2.87×10^{-2}
cdu00730	Thiamine metabolism	7.93×10^{-3}	3.20×10^{-2}
cdu00630	Glyoxylate and dicarboxylate metabolism	8.34×10^{-3}	3.20×10^{-2}
cdu00330	Arginine and proline metabolism	9.61×10^{-3}	3.24×10^{-2}
cdu00670	One carbon pool by folate	9.85×10^{-3}	3.24×10^{-2}

Notes.
padj of < 0.05 set as the significance threshold.

Table 5 Significantly enriched KEGG pathways for genes in RG1, RG2 and UG1.

Sort	KEGG ID	Description	*p*-value	padj
RG1	cdu00190	Oxidative phosphorylation	1.34×10^{-5}	2.27×10^{-4}
RG2	cdu00220	Arginine biosynthesis	1.97×10^{-5}	2.56×10^{-4}
	cdu01130	Biosynthesis of antibiotics	4.09×10^{-3}	2.39×10^{-2}
	cdu01230	Biosynthesis of amino acids	5.52×10^{-3}	2.39×10^{-2}
	cdu01110	Biosynthesis of secondary metabolites	1.21×10^{-2}	3.92×10^{-2}
UG1	cdu00650	Butanoate metabolism	1.82×10^{-2}	4.91×10^{-2}
	cdu00640	Propanoate metabolism	2.48×10^{-2}	4.91×10^{-2}
	cdu00410	beta-Alanine metabolism	2.64×10^{-2}	4.91×10^{-2}
	cdu00280	Valine, leucine and isoleucine degradation	2.81×10^{-2}	4.91×10^{-2}

Notes.
padj of < 0.05 set as the significance threshold.

cell membrane leakage (*Papo & Shai, 2003*; *Paterson et al., 2017*; *Shai, 1999*; *Utesch et al., 2018*). However, mechanistic studies of antimicrobial peptides have determined that their membrane interactions are complex. *Park, Kim & Kim (1998)* showed that buforin II prevents microorganisms entry into cells. *Lee et al. (2019)* found that antifungal β-peptides cause cell death by entering cells and causing nuclear and vacuole dysfunction. *Chileveru et al. (2015)* showed that human alpha-defensin 5 enters the cytoplasm of Escherichia coli and interferes with cell division.

AMPs work through various mechanisms. In our previous studies, we showed that MAF-1A inhibits C. albicans through its effects on the cell wall, cell membrane, and ribosomes (*Wang et al., 2017*). In this study, we found that MAF-1A alters gene expression in several important biological pathways in C. parapsilosis, including oxidation–reduction

Table 6 Significant enriched GO terms of RG1, RG2 and UG2.

Sort	Category	GO ID	Description	*p*-value	padj
RG1	BP	GO:0006091	Generation of precursor metabolites and energy	8.71×10^{-5}	7.14×10^{-3}
	BP	GO:0055114	Oxidation–reduction process	8.49×10^{-4}	3.48×10^{-2}
RG2	BP	GO:0016053	Organic acid biosynthetic process	5.27×10^{-4}	2.11×10^{-2}
	BP	GO:0046394	Carboxylic acid biosynthetic process	5.27×10^{-4}	2.11×10^{-2}
	BP	GO:0044283	Small molecule biosynthetic process	1.56×10^{-3}	3.12×10^{-2}
	BP	GO:0006082	Organic acid metabolic process	2.34×10^{-3}	3.12×10^{-2}
	BP	GO:0019752	Carboxylic acid metabolic process	2.34×10^{-3}	3.12×10^{-2}
	BP	GO:0043436	Oxoacid metabolic process	2.34×10^{-3}	3.12×10^{-2}
UG2	BP	GO:0055114	Oxidation–reduction process	3.53×10^{-4}	2.15×10^{-2}

Notes.
padj of < 0.05 set as the significance threshold for enrichment.

processes and alternative energy sources. We further compared the response of C. albicans and C. parapsilosis to MAF-1A, most DEGs have the same expression trend (upregulated/downregulated), and identified changes in both stress and energy metabolism pathways (carbon metabolism, cell cycle, peroxisome, carbon metabolism, fatty acid degradation) (Tables S3 and S4). We hypothesized that the antifungal peptide MAF-1A exerts antifungal effect and disrupts energy metabolism by affecting oxidation–reduction processes, due to its effects on the mitochondria. Whilst antimicrobial peptides have multiple modes of action, these remain undetermined for MAF-1A. Our findings suggest that intracellular targets may be the key sites of MAF-1A activity, with enrichment analysis of the DEGs suggesting that MAF-1A exerts antimicrobial activity through a variety of mechanisms.

Membrane destruction

Genes with decreased expression after 6 h were significantly enriched in steroid biosynthesis (Fig. 5) including *CpERG1*, *CpERG3*, *CpERG6*, *CpERG7*, *CpERG9*, *CpERG11*, *CpERG25*, *CpERG26*, *CpERG27*, *CpERG2*, *CpERG4*, *CpERG5*, *CpERG24*, and *CpSPBC16A3.12c* (*Kanehisa et al., 2019*; *Ogata et al., 1999*). Azole agents exert antifungal activity by inhibiting the synthesis of ergosterol, a major component of fungal cell membranes (*Ermakova & Zuev, 2017*). The overexpression of *ERG11* (encoding lanosterol 14-demethylase) is a major cause of azole resistance, often mediated by point mutations in the ERG11 gene. Members of the *ERG* gene family encode proteins involved in ergosterol biosynthesis, of which lanosterol 14-demethylase is critical. In this study, MAF-1A decreased the expression of 14 genes related to sterol synthesis including *CpERG11*, suggesting it interferes with ergosterol synthesis. Additionally, 10 genes showed increased expression after 6 h and were enriched in fatty acid degradation pathways (Fig. 6) (*Kanehisa et al., 2019*; *Ogata et al., 1999*). Of these, the expression of *CpPOX4* (CPAR2-807700) significantly increased, (log2 FC = 1.503). We further verified the upregulation of these genes through qRT-PCR (log2FC = 2.834). *CpPOX4* encodes a component of fatty acid biosynthesis, which indicates that the composition of the cell membrane was affected by MAF-1A.

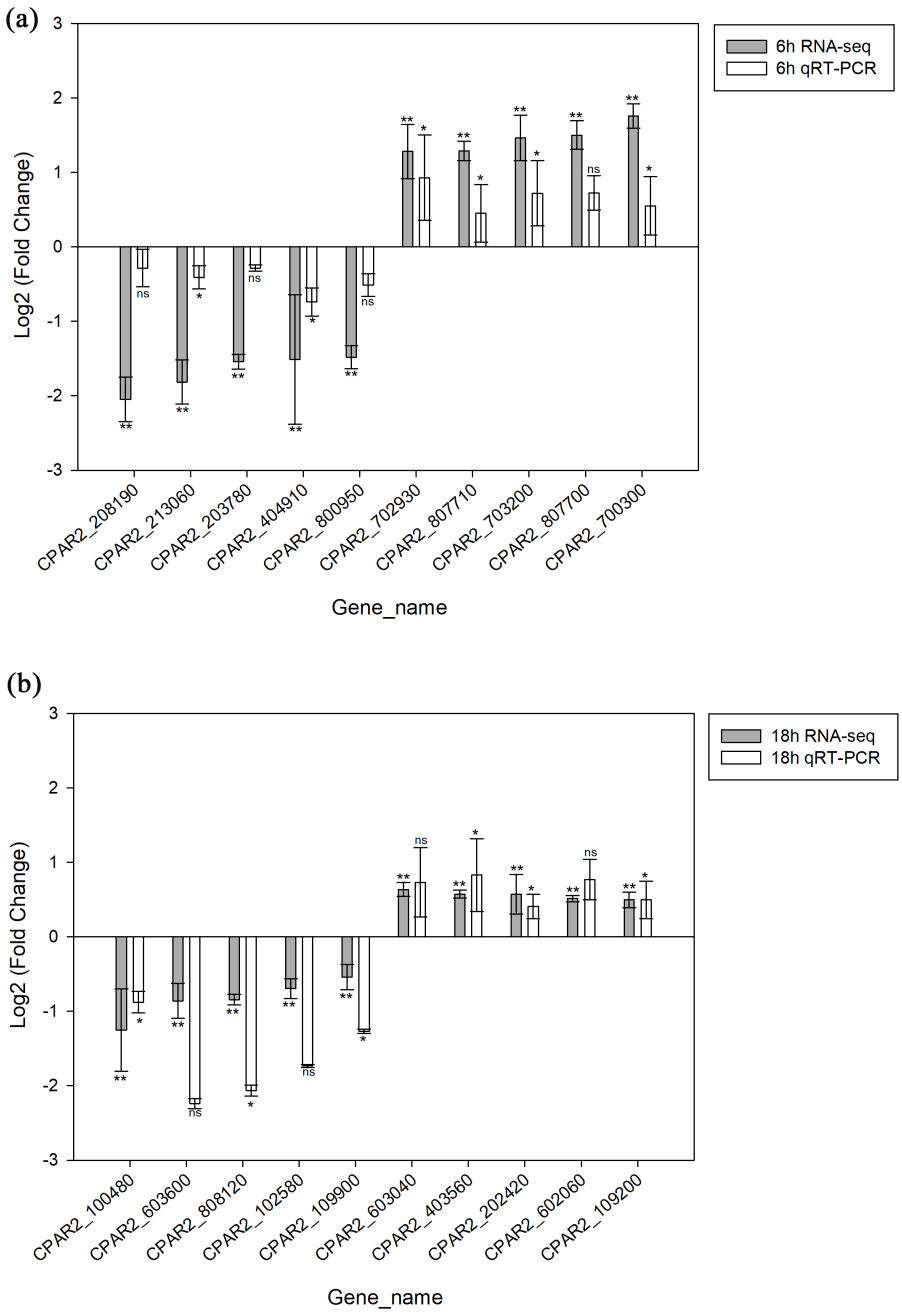

Figure 3 Validation of the RNA-seq data via qRT-PCR analysis. (A) 6 h timepoint. (B) 18 hour timepoint. * $p < 0.05$, ** $p < 0.01$, ns, not-significant.

Full-size DOI: 10.7717/peerj.9767/fig-3

Mitochondrial function

A total of 42 genes showed increased expression at 6 h and were enriched in oxidative phosphorylation pathways. The genes were mainly involved in respiratory chain electron transport processes in the mitochondrial inner membrane, including NHD release of H+ and ATP synthase (Fig. 7) (*Kanehisa et al., 2019*; *Ogata et al., 1999*). A total of six genes

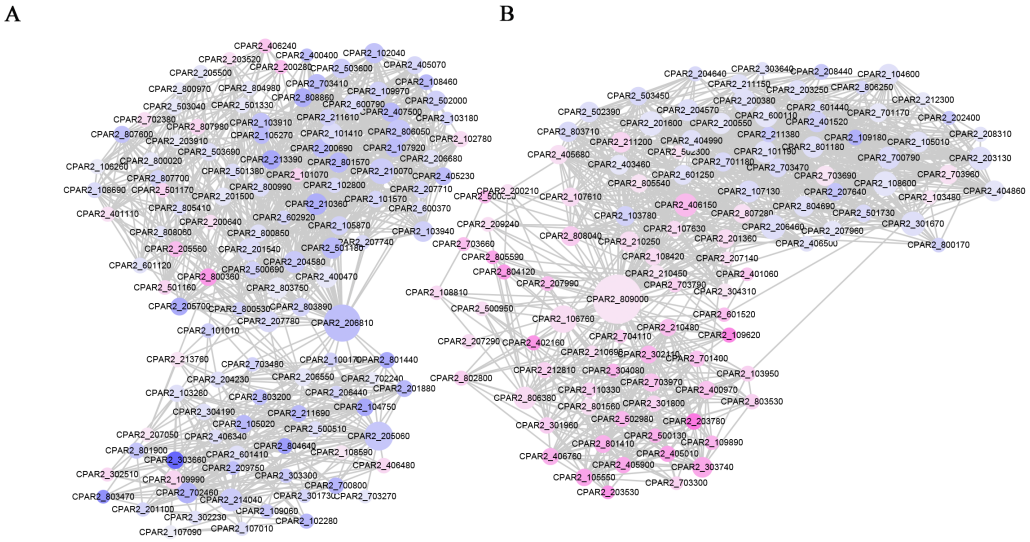

Figure 4 PPI network of the DEGs following MAF-1A treatment of C. parapsilosis for 6 h. Node sizes correlate with node importance; purple nodes denote genes with increased expression, and blue denote decreased expression genes.

Full-size DOI: 10.7717/peerj.9767/fig-4

in RG1 were also enriched in this pathway (*CpCOX15*, *Cpnuo-21*, *CpQCR2*, *CpQCR8*, *CpQCR7*, and *CpCOR1*). Previous studies showed that *COX15* encodes an indispensable mitochondrial protein for Saccharomyces cerevisiae cytochrome oxidase (*Glerum et al., 1997*). Cytochrome oxidase is a terminal enzyme in the respiratory electron transport chain that is essential for ATP synthesis. Reactive oxygen species (ROS) are produced by the oxidative phosphorylation of ATP and can disrupt the electron transport chain in mitochondria (*Piippo et al., 2018*). ROS production induces damage to lipids, proteins, lipids, and nucleic acids, leading to cell death. Eukaryotes prevent cell damage through oxidative stress detoxification and the prevention of ROS accumulation. In this study, GO enrichment analysis of the RG1 genes showed that 7 that were highly expressed were associated with redox processes (*CpPOX9*, *CpCOX15*, *Cpnuo-21*, *CpAAEL001134*, *CpQCR7*, *CpRGI1*, and *CpnamA*). These processes help cells to remove accumulated ROS. Due to the increased expression of these genes in response to MAF-1A, it is possible that MAF-1A promotes oxidative phosphorylation, which disrupts electron transfer in the mitochondria, enhancing ROS production and subsequent cell damage.

C.parapsilosis has an unusual mitochondrial genome architecture, consisting of linear DNA molecules of 30.9-Kbp, terminating with specific telomeric structures on both sides (738-Kbp long). This differs from telomeres at the ends of eukaryotic nuclear chromosomes, particularly in humans (*Kovac, Lazowska & Slonimski, 1984*). MAF-1A interferes with the expression of multiple genes related to the mitochondrial functions of C. parapsilosis, It is, therefore, feasible that MAF-1A interferes with the normal function of C. parapsilosis mitochondria.

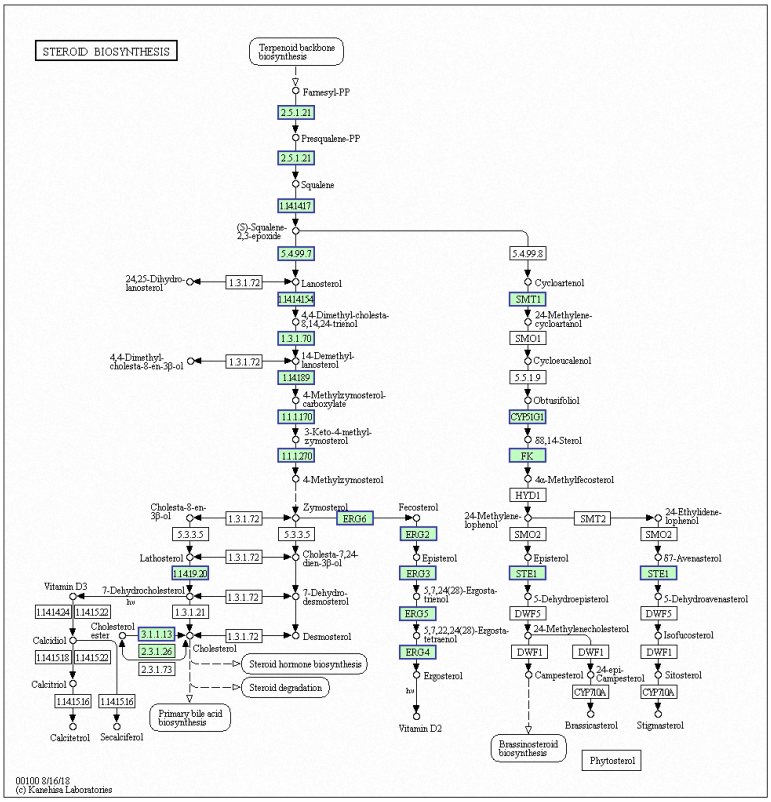

Figure 5 **Significantly enriched KEGG pathways in steroid biosynthesis.** DEGs with decreased expression are shown in blue. Permission for publication granted by the Kyoto Encyclopedia of Genes and Genomes, Kyoto University, Japan.

Full-size DOI: 10.7717/peerj.9767/fig-5

CONCLUSIONS

In summary, MAF-1A has a complex response in C. parapsilosis. Most DEGs identified through RNA-seq analysis were related to oxidation–reduction processes and the use of alternative energy sources, Mitochondria are important target for the anti-fungal peptide MAF-1A to exert anti-C. parapsilosis. RNA-seq data therefore provide future direction to study the antifungal mechanisms of MAF-1A and highlight the potential pathways that contribute to resistance.

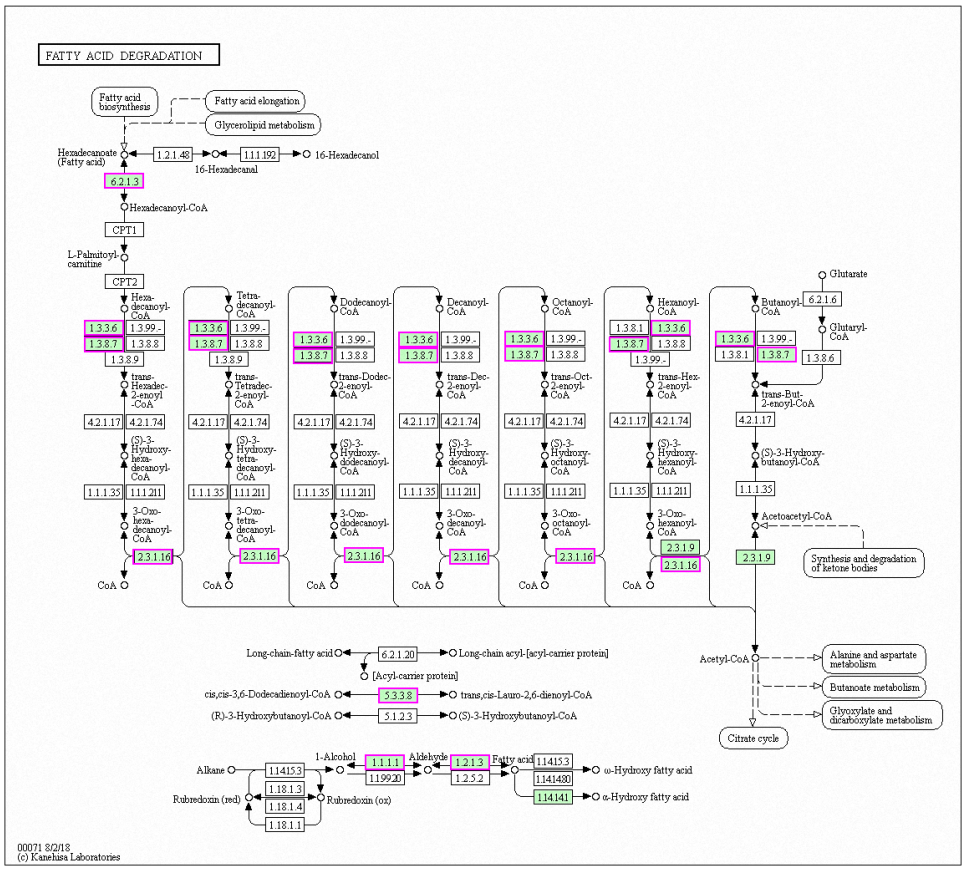

Figure 6 **Significantly enriched KEGG pathways in fatty acid degradation.** DEGs with increased expression are marked in purple. Permission for publication was granted by the Kyoto Encyclopedia of Genes and Genomes, Kyoto University, Japan.

Full-size DOI: 10.7717/peerj.9767/fig-6

ADDITIONAL INFORMATION AND DECLARATIONS

Funding

This work was supported by the Science and Technology Department of Gui Zhou Province ((2019)2827, (2015)4015, (2018)5706); Doctoral Foundation of Guizhou Provincial People's Hospital (GZSYBS(2015)12); Non-profit Central Research Institute Fund of Chinese Academy of Medical Sciences (2019PT320003). The funders had no role in study design, data collection and analysis, decision to publish, or preparation of the manuscript.

Grant Disclosures

The following grant information was disclosed by the authors:
Science and Technology Department of Gui Zhou Province: (2019)2827, (2015)4015, (2018)5706.
Doctoral Foundation of Guizhou Provincial People's Hospital: GZSYBS(2015)12.
Non-profit Central Research Institute Fund of Chinese Academy of Medical Sciences: 2019PT320003.

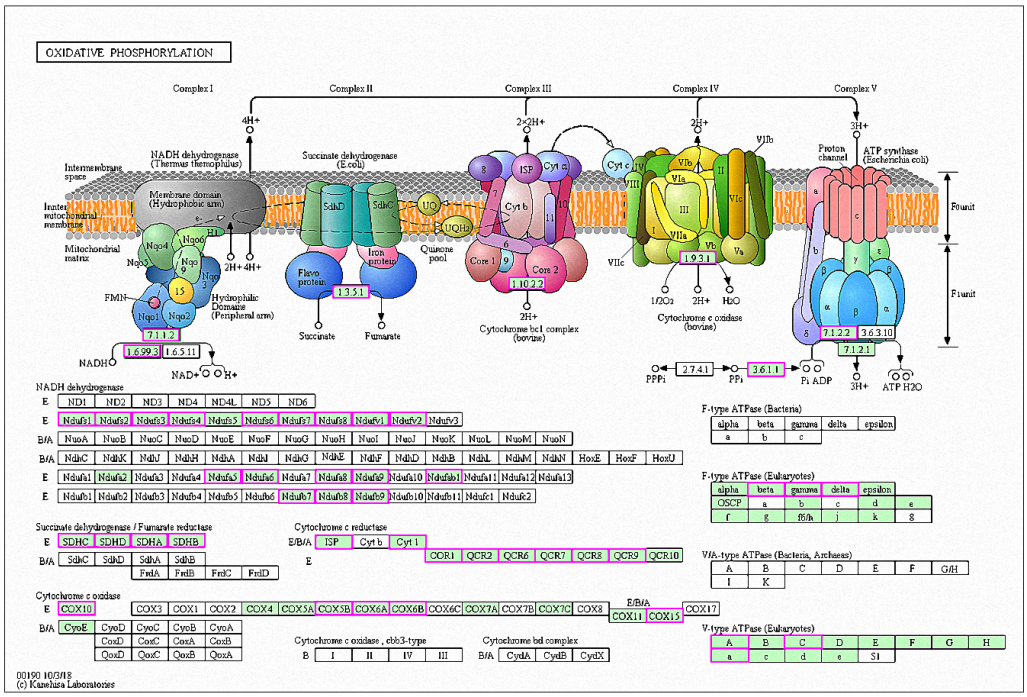

Figure 7 **Significantly enriched KEGG pathways in oxidative phosphorylation.** DEGs with increased expression are marked in purple. Permission for publication was granted by the Kyoto Encyclopedia of Genes and Genomes, Kyoto University, Japan.

Full-size DOI: 10.7717/peerj.9767/fig-7

Competing Interests

The authors declare there are no competing interests.

Author Contributions

- Rong Cheng and Zhenhua Luo conceived and designed the experiments, performed the experiments, analyzed the data, prepared figures and/or tables, authored or reviewed drafts of the paper, and approved the final draft.
- Wei Li performed the experiments, prepared figures and/or tables, and approved the final draft.
- Klarke M. Sample conceived and designed the experiments, analyzed the data, prepared figures and/or tables, and approved the final draft.
- Qiang Xu performed the experiments, authored or reviewed drafts of the paper, and approved the final draft.
- Lin Liu, Fuxun Yu and Yingjie Nie analyzed the data, authored or reviewed drafts of the paper, and approved the final draft.
- Xiangyan Zhang conceived and designed the experiments, prepared figures and/or tables, and approved the final draft.

Data Availability

The following information was supplied regarding data availability:

The raw data are available in the Supplementary File.

Supplemental Information

Supplemental information for this article can be found online at http://dx.doi.org/10.7717/peerj.9767#supplemental-information.

REFERENCES

Benjamini Y, Drai D, Elmer G, Kafkafi N, Golani I. 2001. Controlling the false discovery rate in behavior genetics research. *Behavioural Brain Research* **125**:279–284.

Chileveru HR, Lim SA, Chairatana P, Wommack AJ, Chiang IL, Nolan EM. 2015. Visualizing attack of Escherichia coli by the antimicrobial peptide human defensin 5. *Biochemistry* **54**:1767–1777 DOI 10.1021/bi501483q.

Ermakova E, Zuev Y. 2017. Effect of ergosterol on the fungal membrane properties. All-atom and coarse-grained molecular dynamics study. *Chemistry and Physics of Lipids* **209**:45–53 DOI 10.1016/j.chemphyslip.2017.11.006.

Fais R, Di Luca M, Rizzato C, Morici P, Bottai D, Tavanti A, Lupetti A. 2017. The N-terminus of human lactoferrin displays anti-biofilm activity on candida parapsilosis in lumen catheters. *Frontiers in Microbiology* **8**:Article 2218 DOI 10.3389/fmicb.2017.02218.

Fu P, Wu J, Guo G. 2009. Purification and molecular identification of an antifungal peptide from the hemolymph of Musca domestica (housefly). *Cellular & Molecular Immunology* **6**:245–251 DOI 10.1038/cmi.2009.33.

Ghosh C, Sarkar P, Issa R, Haldar J. 2019. Alternatives to conventional antibiotics in the era of antimicrobial resistance. *Trends in Microbiology* **27**:323–338 DOI 10.1016/j.tim.2018.12.010.

Glerum DM, Muroff I, Jin C, Tzagoloff A. 1997. COX15 codes for a mitochondrial protein essential for the assembly of yeast cytochrome oxidase. *Journal of Biological Chemistry* **272**:19088–19094 DOI 10.1074/jbc.272.30.19088.

Guilhelmelli F, Vilela N, Albuquerque P, Derengowski Lda S, Silva-Pereira I, Kyaw CM. 2013. Antibiotic development challenges: the various mechanisms of action of antimicrobial peptides and of bacterial resistance. *Frontiers in Microbiology* **4**:Article 353 DOI 10.3389/fmicb.2013.00353.

Holland LM, Schroder MS, Turner SA, Taff H, Andes D, Grozer Z, Gacser A, Ames L, Haynes K, Higgins DG, Butler G. 2014. Comparative phenotypic analysis of the major fungal pathogens Candida parapsilosis and Candida albicans. *PLOS Pathogens* **10**:e1004365 DOI 10.1371/journal.ppat.1004365.

Huber A, Galgóczy L, Váradi G, Holzknecht J, Kakar A, Malanovic N, Leber R, Koch J, Keller MA, Batta G, Tóth GK, Marx F. 2020. Two small, cysteine-rich and cationic antifungal proteins from Penicillium chrysogenum: a comparative study of PAF and PAFB. *Biochimica et Biophysica Acta—Biomembranes* **1862(8)**:Article 183246 DOI 10.1016/j.bbamem.2020.183246.

Iracane E., Donovan PD., Ola M., Butler G., Holland LM.. 2018. Identification of an exceptionally long intron in the HAC1 gene of Candida parapsilosis. *mSphere* **3(6)**:e00532–18.

Kanehisa M, Sato Y, Furumichi M, Morishima K, Tanabe M. 2019. New approach for understanding genome variations in KEGG. *Nucleic Acids Research* **47**:D590–D595 DOI 10.1093/nar/gky962.

Kim D, Langmead B, Salzberg SL. 2015. HISAT: a fast spliced aligner with low memory requirements. *Nature Methods* **12**:357–360 DOI 10.1038/nmeth.3317.

Kobbi S, Nedjar N, Chihib N, Balti R, Chevalier M, Silvain A, Chaabouni S, Dhulster P, Bougatef A. 2018. Synthesis and antibacterial activity of new peptides from Alfalfa RuBisCO protein hydrolysates and mode of action via a membrane damage mechanism against Listeria innocua. *Microbial Pathogenesis* **115**:41–49 DOI 10.1016/j.micpath.2017.12.009.

Kovac L, Lazowska J, Slonimski P. 1984. A yeast with linear molecules of mitochondrial DNA. *Molecular and General Genetics* **197**:420–424.

Lee MR, Raman N, Ortiz-Bermudez P, Lynn DM, Palecek SP. 2019. 14-helical beta-peptides elicit toxicity against C. albicans by forming pores in the cell membrane and subsequently disrupting intracellular organelles. *Cell Chemical Biology* **26**:289–299. e284 DOI 10.1016/j.chembiol.2018.11.002.

Li L, Song F, Sun J, Tian X, Xia S, Le G. 2016. Membrane damage as first and DNA as the secondary target for anti-candidal activity of antimicrobial peptide P7 derived from cell-penetrating peptide ppTG20 against Candida albicans. *Journal of Peptide Science* **22**:427–433 DOI 10.1002/psc.2886.

Li Y, Sun S, Guo Q, Ma L, Shi C, Su L, Li H. 2008. In vitro interaction between azoles and cyclosporin A against clinical isolates of Candida albicans determined by the chequerboard method and time-kill curves. *Journal of Antimicrobial Chemotherapy* **61**:577–585 DOI 10.1093/jac/dkm493.

Lis M, Liu TT, Barker KS, Rogers PD, Bobek LA. 2010. Antimicrobial peptide MUC7 12-mer activates the calcium/calcineurin pathway in Candida albicans. *FEMS Yeast Research* **10**:579–586 DOI 10.1111/j.1567-1364.2010.00638.x.

Livak KJ, Schmittgen TD. 2001. Analysis of relative gene expression data using real-time quantitative PCR and the 2(−Delta Delta $C(T)$) Method. *Methods* **25**:402–408 DOI 10.1006/meth.2001.1262.

Lotfali E, Kordbacheh P, Mirhendi H, Zaini F, Ghajari A, Mohammadi R, Noorbakhsh F, Moazeni M, Fallahi A, Rezaie S. 2016. Antifungal susceptibility analysis of clinical isolates of Candida parapsilosis in Iran. *Iranian Journal of Public Health* **45**:322–328.

Love MI, Huber W, Anders S. 2014. Moderated estimation of fold change and dispersion for RNA-seq data with DESeq2. *Genome Biology* **15**:Article 550 DOI 10.1186/s13059-014-0550-8.

Maria S, Barnwal G, Kumar A, Mohan K, Vinod V, Varghese A, Biswas R. 2018. Species distribution and antifungal susceptibility among clinical isolates of Candida parapsilosis complex from India. *Revista Iberoamericana de Micologia* **35**:147–150 DOI 10.1016/j.riam.2018.01.004.

Moravej H, Moravej Z, Yazdanparast M, Heiat M, Mirhosseini A, Moosazadeh Moghaddam M, Mirnejad R. 2018. Antimicrobial peptides: features, action, and

their resistance mechanisms in bacteria. *Microbial Drug Resistance* **24**:747–767 DOI 10.1089/mdr.2017.0392.

Mortazavi A, Williams BA, McCue K, Schaeffer L, Wold B. 2008. Mapping and quantifying mammalian transcriptomes by RNA-Seq. *Nature Methods* **5**:621–628 DOI 10.1038/nmeth.1226.

Nuti R, Goud NS, Saraswati AP, Alvala R, Alvala M. 2017. Antimicrobial peptides: a promising therapeutic strategy in tackling antimicrobial resistance. *Current Medicinal Chemistry* **24**:4303–4314 DOI 10.2174/0929867324666170815102441.

Ogata H, Goto S, Sato K, Fujibuchi W, Bono H, Kanehisa M. 1999. KEGG: kyoto encyclopedia of genes and genomes. *Nucleic Acids Research* **27**:29–34 DOI 10.1093/nar/27.1.29.

Papo N, Shai Y. 2003. Exploring peptide membrane interaction using surface plasmon resonance: differentiation between pore formation versus membrane disruption by lytic peptides. *Biochemistry* **42**:458–466 DOI 10.1021/bi0267846.

Park CB, Kim HS, Kim SC. 1998. Mechanism of action of the antimicrobial peptide buforin II: buforin II kills microorganisms by penetrating the cell membrane and inhibiting cellular functions. *Biochemical and Biophysical Research Communications* **244**:253–257 DOI 10.1006/bbrc.1998.8159.

Paterson DJ, Tassieri M, Reboud J, Wilson R, Cooper JM. 2017. Lipid topology and electrostatic interactions underpin lytic activity of linear cationic antimicrobial peptides in membranes. *Proceedings of the National Academy of Sciences of the United States of America* **114**:E8324–E8332 DOI 10.1073/pnas.1704489114.

Patocka J, Nepovimova E, Klimova B, Wu Q, Kuca K. 2018. Antimicrobial peptides: amphibian host defense peptides. *Current Medicinal Chemistry* **26(32)**:5924–5946 DOI 10.2174/0929867325666180713125314.

Piippo N, Korhonen E, Hytti M, Kinnunen K, Kaarniranta K, Kauppinen A. 2018. Oxidative stress is the principal contributor to inflammasome activation in retinal pigment epithelium cells with defunct proteasomes and autophagy. *Cellular Physiology and Biochemistry* **49**:359–367 DOI 10.1159/000492886.

Robbins N, Caplan T, Cowen LE. 2017. Molecular evolution of antifungal drug resistance. *Annual Review of Microbiology* **71**:753–775 DOI 10.1146/annurev-micro-030117-020345.

Shai Y. 1999. Mechanism of the binding, insertion and destabilization of phospholipid bilayer membranes by alpha-helical antimicrobial and cell non-selective membrane-lytic peptides. *Biochimica et Biophysica Acta/General Subjects* **1462**:55–70.

Shannon P, Markiel A, Ozier O, Baliga NS, Wang JT, Ramage D, Amin N, Schwikowski B, Ideker T. 2003. Cytoscape: a software environment for integrated models of biomolecular interaction networks. *Genome Research* **13**:2498–2504 DOI 10.1101/gr.1239303.

Sular FL, Szekely E, Cristea VC, Dobreanu M. 2018. Invasive fungal infection in Romania: changing incidence and epidemiology during six years of surveillance in a tertiary hospital. *Mycopathologia* **183**:967–972 DOI 10.1007/s11046-018-0293-2.

Sun S, Li Y, Guo Q, Shi C, Yu J, Ma L. 2008. In vitro interactions between tacrolimus and azoles against Candida albicans determined by different methods. *Antimicrobial Agents and Chemotherapy* **52**:409–417 DOI 10.1128/AAC.01070-07.

Thomaz DY, De Almeida Jr JN, Lima GME, Nunes MO, Camargo CH, Grenfell RC, Benard G, Negro GMBDel. 2018. An azole-resistant Candida parapsilosis outbreak: clonal persistence in the intensive care unit of a brazilian teaching hospital. *Frontiers in Microbiology* **9**:Article 2997 DOI 10.3389/fmicb.2018.02997.

Toth R, Nosek J, Mora-Montes HM, Gabaldon T, Bliss JM, Nosanchuk JD, Turner SA, Butler G, Vagvolgyi C, Gacser A. 2019. Candida parapsilosis: from genes to the bedside. *Clinical Microbiology Reviews* **32**(**2**):e00111–18 DOI 10.1128/cmr.00111-18.

Utesch T, De Miguel Catalina A, Schattenberg C, Paege N, Schmieder P, Krause E, Miao Y, McCammon JA, Meyer V, Jung S, Mroginski MA. 2018. A computational modeling approach predicts interaction of the antifungal protein AFP from Aspergillus giganteus with fungal membranes via its gamma-core motif. *mSphere* **3**:e00377–18 DOI 10.1128/mSphere.00377-18.

Vieira de Melo AP, Zuza-Alves DL, Da Silva-Rocha WP, Ferreira Canario de Souza LB, Francisco EC, Salles de Azevedo Melo A, Maranhao Chaves G. 2019. Virulence factors of Candida spp. obtained from blood cultures of patients with candidemia attended at tertiary hospitals in Northeast Brazil. *Journal de Mycologie Medicale* **29**(**2**):132–139 DOI 10.1016/j.mycmed.2019.02.002.

Wang T, Xiu J, Zhang Y, Wu J, Ma X, Wang Y, Guo G, Shang X. 2017. Transcriptional responses of Candida albicans to antimicrobial peptide MAF-1A. *Frontiers in Microbiology* **8**:Article 894 DOI 10.3389/fmicb.2017.00894.

Yu G, Wang LG, Han Y, He QY. 2012. clusterProfiler: an R package for comparing biological themes among gene clusters. *Omics* **16**:284–287 DOI 10.1089/omi.2011.0118.

Zhou J, Kong L, Fang N, Mao B, Ai H. 2016. Synthesis and functional characterization of maf-1a peptide derived from the larvae of housefly, Musca domestica (Diptera: Muscidae). *Journal of Medical Entomology* **53**:1467–1472 DOI 10.1093/jme/tjw110.